



ELSEVIER

Available online at www.sciencedirect.com

SCIENCE @ DIRECT®

Combustion and Flame 136 (2004) 168–179

Combustion
and Flame

www.elsevier.com/locate/jnlabr/cnf

Ignition of premixed hydrogen/air by heated counterflow under reduced and elevated pressures

X.L. Zheng and C.K. Law*

Department of Mechanical and Aerospace Engineering, Princeton University, Princeton, NJ 08544, USA

Received 25 April 2003; received in revised form 1 September 2003; accepted 1 September 2003

Abstract

The temperature of an inert jet required to ignite a counterflowing lean premixed hydrogen/air jet was experimentally determined over the pressure range of 0.6 to 7 atm and computationally simulated using detailed chemistry and transport. Results show that, compared to the homogeneous explosion limits, ignition takes place at higher temperatures and exhibits five limits over the pressure range investigated. The first and second ignition limits resemble the corresponding first and second homogeneous explosion limits, except they have steeper slopes in the pressure–temperature response, with the first limit being affected by the significant transport loss of the H radical and the second limit modified by the activation of the otherwise metastable HO₂ radicals by the diffusively enriched H₂. The third and fifth ignition limits are respectively manifestations of the low- and high-pressure responses of the third homogeneous explosion limit behavior, which is nevertheless punctuated by the fourth ignition limit characterized by the HO₂–H reactions. Furthermore, the fourth ignition limit runs fairly parallel to the crossover temperature, but is shifted to lower temperatures. An explicit expression, $2k_1 = \{2k_{10}/(k_{10} + k_{11})\}k_9[M]$, was derived and found to describe well this limit as well as the extended second limit observed in previous flow reactor studies. It is further shown that, since transport effects are inherently important for the present premixed system because of the diffusive loss of H to the hot, inert side of the counterflow, the ignition temperature increases substantially with increasing strain rate at all pressures and that such a sensitivity can be moderated by doping the inert flow with a small amount of oxygen.

© 2003 The Combustion Institute. Published by Elsevier Inc. All rights reserved.

Keywords: Hydrogen chemistry; Ignition; Extended second limit

1. Introduction

The chemical kinetics of the H₂/O₂ system has been extensively studied [1–5], yielding results that have enabled investigations of the combustion characteristics of H₂/O₂ mixtures in various physical environments. Of particular relevance to the present study is the series of computational, experimental, and analytical investigations [6–13] on the forced nonpremixed ignition of a cold hydrogen/nitrogen

jet by a counterflowing heated air jet. These studies yielded the interesting result [10,11] that the ignition response in this convective–diffusive system qualitatively mimics the homogeneous system in that the ignition boundary, in terms of the system pressure and temperature, follows closely the Z-shaped explosion limits of the homogeneous H₂/O₂ mixture. The effect of aerodynamic straining is simply a displacement of the Z curve along the line of the crossover temperature. Consequently, for a given pressure, the ignition temperature in the second limit is remarkably insensitive to the applied strain rate. Indeed, since the H₂/O₂ system is so chemically reactive, the rates of the key elementary reactions are several orders larger

* Corresponding author.

E-mail address: cklaw@princeton.edu (C.K. Law).

than those of convection and diffusion such that kinetically controlled ignition events were also observed for some first- and third-limit situations that are close to the second limit. These results were interpreted on the basis of ignition occurring in an ignition kernel, situated in the hot region of the flow, within which the reaction rates as well as the concentrations of the key intermediate species both attain their respective peak values.

The above studies on nonpremixed ignition were subsequently extended to premixed ignition in which a cold premixed H_2 /air jet is ignited by an impinging, hot inert jet [14]. The phenomena turned out to be substantially richer than anticipated, embodying new understanding of ignition which is unique to the premixed system. Specifically, since hydrogen diffuses much faster than oxygen, the composition of the flow becomes stratified as both reactants diffuse toward the ignition kernel, which is located on the hot, inert side of the flow. This results in a fuel-rich mixture in the ignition kernel even for a very lean free-stream mixture. The dearth of oxygen in the kernel then reduces the production rates of the key reaction intermediates to levels comparable to their diffusive loss rates from the kernel, causing the premixed ignition temperature to be substantially higher than the nonpremixed ignition temperature. The influence of the strain rate is correspondingly increased. It was further demonstrated that this increased difficulty in ignition can be partly mitigated by doping the inert flow with a small quantity of oxygen, which in effect instills a nonpremixed character to the system.

The study of Ref. [14] was conducted at atmospheric pressure. Since ignition phenomena are inherently chemistry sensitive, and since such sensitivity is strongly manifested in terms of pressure variations for the H_2/O_2 system, we have extended the study to situations at reduced and elevated pressures. We shall show in due course that the ignition response is further enriched as the system pressure is traversed, yielding useful insight into the effects of pressure on chemistry–transport coupling in general and the efficiencies of chain mechanisms in particular.

In the following, we shall first present the experimental and computational methodologies and then examine effects of pressure, strain rate, and oxygen addition to the hot, inert side of the flow on the system ignition.

2. Experimental and computational specifications

The pressurized burner used in previous nonpremixed counterflow ignition experiments [9] was adapted for the present study. The upper part of the counterflow was formed by a nitrogen jet, with

or without oxygen doping, from a 20-mm-diameter quartz tube, while the lower part was a hydrogen/air mixture issuing from another 20-mm quartz tube. The tubes were separated by 20 mm and were surrounded by nitrogen coflows. A silicon carbide heater was placed in the upper flow and the temperature was regulated using a proportional-integral-derivative temperature controller. The entire burner tube assembly was housed within a pressurized chamber filled with nitrogen. Temperature and velocity fields in the axial direction between the burner tubes were respectively measured by a bare K-type thermocouple (0.003-in.-diameter wire) and a two-component laser Doppler velocimetry (LDV) system.

Data were collected in flows with the stagnation surface located near the midpoint of the flow field, with the inert nitrogen temperature slowly raised until a flame appeared. The hydrogen fuel was doped with a trace amount of methane to make the flame visible. To ensure that the doping did not affect the ignition temperature itself, some experiments were repeated without methane and ignition was alternately monitored by a sudden increase in the chamber pressure.

Upon achieving ignition, the fuel concentration was reduced until the flame disappeared and the peak temperature at the oxidizer exit was measured by an external thermocouple. This temperature was corrected for radiation loss according to Ref. [9] and was considered to be the ignition temperature. It had an absolute uncertainty of up to ± 20 K due to: (1) uncertainty about which model of the gas flow around the thermocouple bead, e.g., a sphere vs a cylinder in cross-flow, best describes the actual shape of the bead, and (2) uncertainty in the radiation calculation [9]. To determine the velocity characteristics of the system, the oxidizer temperature was reduced 5–10 K below the value at ignition before the LDV measurements were performed.

Laminar ignition calculations were performed with the code of Kreutz and Law [10], with detailed transport and chemistry, using the reaction mechanism of Mueller et al. [5]. The calculations determined steady-state solutions at different hot boundary temperatures assuming potential flow, with the velocity gradient given by the experimentally measured value. The ignition temperature was found by determining the boundary temperature at the lower turning point of the ignition–extinction S curve. We note in passing that it was shown and discussed in Ref. [9] that since ignition is mainly governed by the local velocity gradient immediately upstream of the mixing layer on the oxidizer side, the use of the simpler potential flow formulation adequately describes the ignition characteristics.

3. Results and discussion

3.1. Effects of pressure

As a reference to subsequent discussion of the response of the ignition temperature in the present premixed counterflow system, we plot in Fig. 1 the characteristic Z-shaped pressure–temperature explosion limits of a homogeneous mixture, which in this case is stoichiometric in composition and is contained in a spherical KCl-coated vessel of 7.4 cm diameter [1]. It is well established [15] that explosion of the homogeneous mixture is governed by a balance between chain branching and wall termination in the first limit; by the competition between branching, $\text{H} + \text{O}_2 \rightarrow \text{O} + \text{OH}$, and the destruction of H through $\text{H} + \text{O}_2 + \text{M} \rightarrow \text{HO}_2 + \text{M}$ in the second limit; and through reactions involving HO_2 and H_2O_2 in the third limit.

Figure 1 shows the ignition temperatures determined from both calculation and experiment for 9% H_2 in air ($\phi = 0.236$) versus heated N_2 at a pressure-weighted strain rate [9,10] of $k = 216 \text{ s}^{-1}$. It is first noted that the experimental and calculated values agree closely with each other within 10 K. This level of agreement exists for almost all the results reported in the present study, with the only exception being the 3% O_2 case of Fig. 16, which shows slightly larger deviations of about 20 K at higher pressures.

Comparing the counterflow ignition and homogeneous explosion results, it is seen that, while the counterflow response mimics the homogeneous limits in some aspects, it is more complex and is characterized by fundamental differences. First of all, the coun-

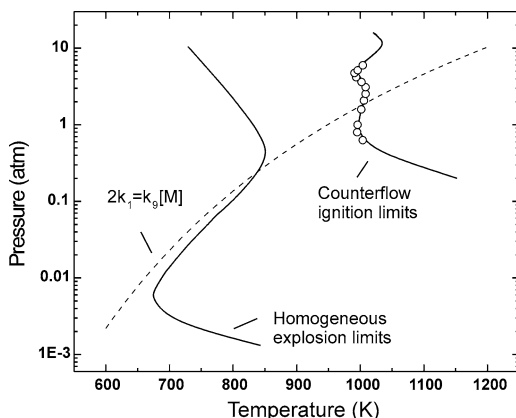


Fig. 1. Comparison between the pressure–temperature explosion limits of a stoichiometric homogeneous H_2/O_2 mixture and the ignition limits of an H_2/air flow by a counterflowing at a pressure-weighted strain rate k of 216 s^{-1} . For the counterflow results, symbols are experimental and line is computational.

terflow ignition response curve is shifted to higher temperatures compared to that of the homogeneous explosion limits. Second, compared to the three explosion limits of the homogeneous mixture, it has five branches, which we shall call the first, second, third, fourth, and fifth ignition limits in the direction of increasing pressure, in order to draw correspondence with the homogeneous case. These five ignition limits have the following characteristics. In the first and second limits the ignition temperature decreases and increases with increasing pressure, respectively, similar to the behavior of the corresponding first and second homogeneous explosion limits. However, the second ignition limit now terminates around 3 atm and the response reverses trend such that the ignition temperature decreases again with increasing pressure over the range of 3–5 atm, which constitutes the third ignition limit. The ignition curve subsequently turns again to form a segment corresponding to the fourth ignition limit. This limit is somewhat parallel to the crossover temperature, defined by $2k_1 = k_9[\text{M}]$, but is shifted to lower temperatures for given pressures. The final reversal yields the fifth limit over which ignition becomes easier again with increasing pressure. This limit was obtained only through calculations because the pressure range is too high for the present experimental setup.

Before discussing in detail the various chemical and physical factors controlling the five limits, some basic characteristics associated with the premixed system need to be addressed in advance because they govern the ignition behavior for all pressures. The general structure of the ignition kernel, defined as the location of the highest reactivity, is shown in Fig. 2, in which spatially resolved profiles of temperature and species concentrations are plotted for the ignition state when $T_{\text{ign}} = 996.5 \text{ K}$ at 1 atm. These profiles highlight the unique features of premixed ignition. As briefly mentioned earlier, since hydrogen is more mobile than oxygen, it diffuses farther toward the inert stream. This yields a stratified distribution of hydrogen and oxygen, with the ignition kernel being substantially more fuel rich than the free stream of the premixed flow. Furthermore, since there is no oxygen from the hot free stream to react with the highly diffusive H radicals, these radicals will leak out of the ignition kernel, as shown by the long tail extending to the hot boundary in Fig. 2. These two features play prominent roles in modifying the three homogeneous explosion limits to the five ignition limits of the present diffusion-affected system, to be discussed next.

3.1.1. The first limit

The first ignition limit is identified in Fig. 1 as the lowest pressure regime in which the ignition tempera-

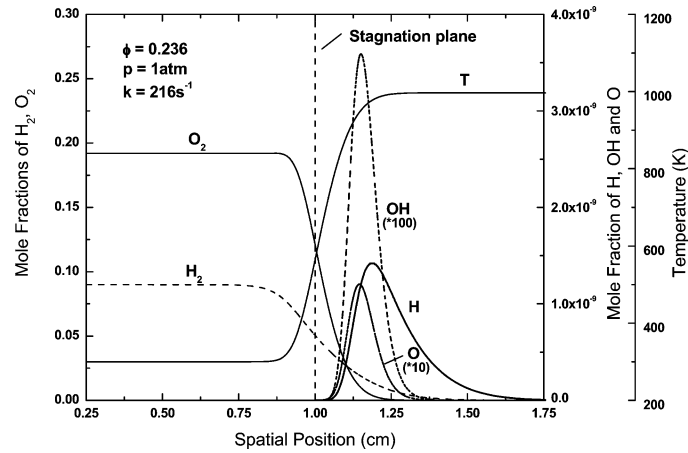


Fig. 2. Major (H_2 , O_2) and minor (H , OH , and O) species concentration and temperature profiles at 1 atm.

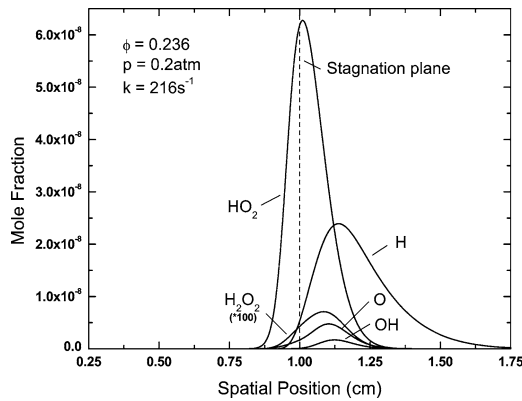


Fig. 3. Minor (H , O , OH , HO_2 , and H_2O_2) species concentrations profiles at 0.2 atm.

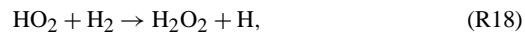
ture increases with decreasing pressure. Similar to the homogeneous case, the diffusive loss of radicals relative to their production becomes progressively more important with reducing pressure, as demonstrated by the substantially broadened profiles of H , O , and OH in Fig. 3, in which the spatial distributions of the minor species at 0.2 atm are plotted at the ignition state. These radicals back-diffuse across the stagnation plane into the premixed stream, far away from the peak location of the H radical which marks the center of the ignition kernel. The spatial distributions of elementary reaction rates (Fig. 4) also show that the production and destruction rates of H are not balanced within the ignition kernel, and some H radicals generated are lost by diffusion.

It is necessary to emphasize the difference between the diffusive loss in the first limit and the H radical loss to the hot, inert stream for all limits. At the first ignition limit, the diffusive loss of the H , O , and OH radicals out of the ignition kernel and across the stagnation plane is characteristic only of low-pressure

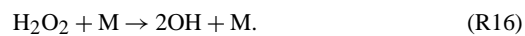
ignition, for which diffusion becomes significant relative to reaction. As pressure increases, this mode of diffusive loss becomes negligible, as shown in Fig. 2, in which the H , O , and OH profiles at 1 atm have narrow peaks and do not penetrate across the stagnation plane. However, the leakage of H to the hot boundary exists at all pressure ranges and is intrinsic to premixed ignition with the hot ignition source being inert.

3.1.2. The second and third ignition limits

As pressure increases, the inhibitive effect of the diffusive loss is taken over by the three-body reaction (R9): $\text{H} + \text{O}_2 + \text{M} \rightarrow \text{HO}_2 + \text{M}$, which effectively competes with the chain-branching reaction (R1): $\text{H} + \text{O}_2 \rightarrow \text{OH} + \text{O}$. While this consideration is the same as that for the *homogeneous* second explosion limit, there is an additional consideration for the present premixed ignition. That is, there is now a relative abundance of H_2 in the ignition kernel due to its preferential diffusion over O_2 . Consequently before the HO_2 radicals are swept out of the ignition kernel, they encounter the abundant H_2 and react with them through



which converts the otherwise inactive HO_2 to the more reactive H radicals. Figure 5 shows that the contribution to H radicals from (R18) is almost comparable to that from the chain-branching reaction (R2): $\text{O} + \text{H}_2 \rightarrow \text{H} + \text{OH}$. Moreover, some of the H_2O_2 radicals generated by (R18) are able to further decompose to two OH through



Consequently, the net effect of the above two reactions is to convert one relatively inert HO_2 to three

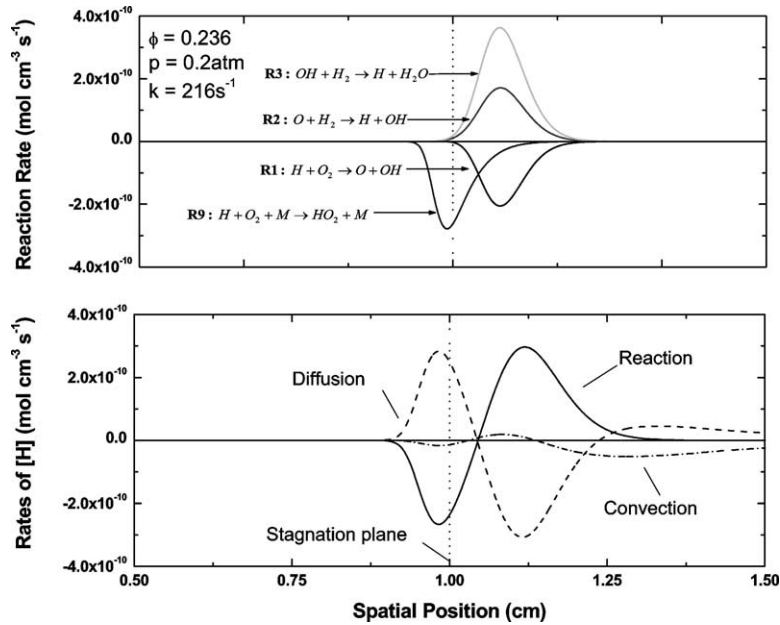


Fig. 4. Spatially resolved rates for hydrogen radical production, destruction, and mass transport (mol cm⁻³ s⁻¹) at 0.2 atm. Top: Rates of individual elementary reactions. Bottom: Rates of diffusive and convective transport compared with the overall chemical production rate for H.

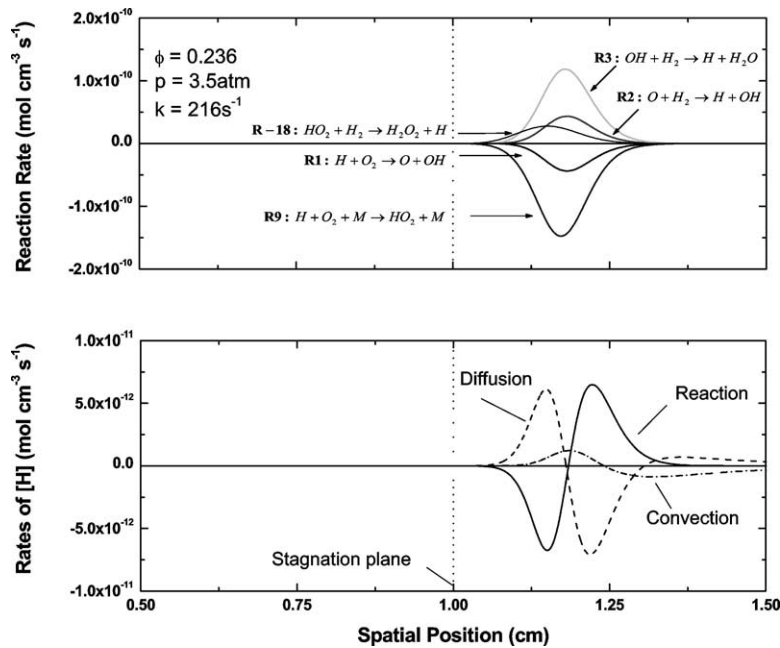


Fig. 5. Spatially resolved rates for hydrogen radical production, destruction, and mass transport (mol cm⁻³ s⁻¹) at 3.5 atm. Top: Rates of individual elementary reactions. Bottom: Rates of diffusive and convective transport compared with the overall chemical production rate for H.

more reactive radicals. All these effects then act in concert to render the increased generation of HO₂ from (R9) with increasing pressure to be a facilitating instead of a retarding reaction. Consequently, the

second limit in the p - T space is steepened and finally turns around at about 3 atm to form the third limit.

The above discussion is further supported by a sensitivity analysis of the S curve, which determines

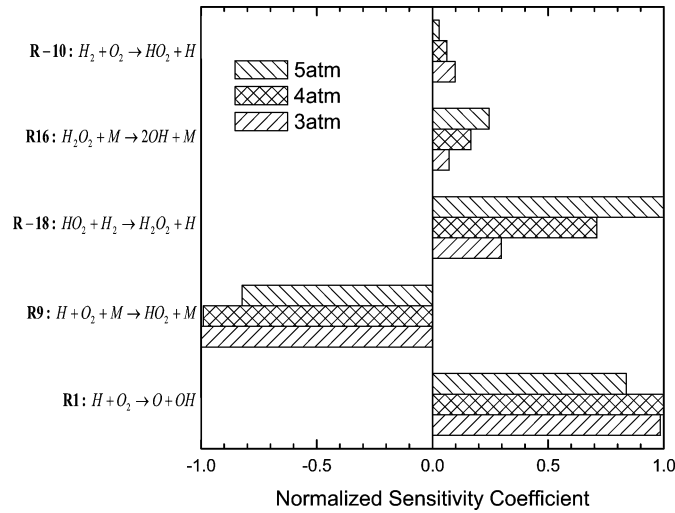


Fig. 6. Sensitivity of the S curve to individual reaction rates normalized by the largest value at 3, 4, and 5 atm. Conditions: heated N_2 flowing against a cold mixture of 9% H_2 in air ($\phi = 0.236$) and $k = 216 \text{ s}^{-1}$.

its response in a region close to the ignition turning point to a perturbation in each of the reaction rates, i.e.,

$$\frac{\partial \ln[X_H]_{\max}}{\partial \ln A_i}$$

where $[X_H]_{\max}$ is the maximum mole fraction of the hydrogen radical, and A_i is the pre-exponential factor for the i th reaction rate constant [11]. It is seen in Fig. 6 that, with increasing pressure, (R18) and (R16) become progressively more important, accompanied by a weakening of the termination effect of (R9).

3.1.3. The fourth ignition limit

By further increasing the pressure, a fourth ignition limit appears at which ignition again becomes more difficult (Fig. 1). Figure 7 shows the system response represented by the maximum H concentration to the hot boundary temperature at 1, 5, and 8 atm, which lie respectively in the second, third, and fourth ignition limits. These curves indicate that the ignition states at 8 atm are qualitatively different from the other two. That is, at 1 and 5 atm, the maximum mole fractions of H at the ignition, turning-point, states are only around 10^{-9} . However, when the pressure is progressively increased, the ignition turning point gradually evolves to an inflection point and then finally disappears. Simultaneously, another ignition turning point emerges with a higher H concentration, say about 10^{-5} at 8 atm.

To identify the processes that govern ignition at the fourth ignition limit, a series of flux analyses for different species under various pressures were performed. It was found that the H radicals generated

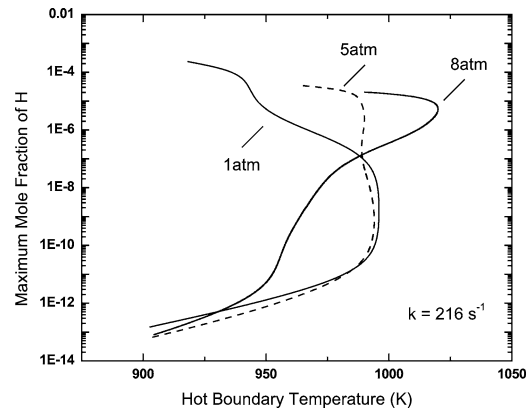


Fig. 7. Calculated S curves for H_2 /air mixtures at three different pressures.

from (R18) now actively react with HO_2 through



Thus (R10) not only competes with (R18) for the HO_2 radical, which could produce an H radical through (R18), but it also consumes the H radical produced by (R18). Furthermore, it is chain terminating. On the other hand, (R11) is chain branching if HO_2 is considered inert. The ignition behavior is therefore modified by their competition, as will be discussed shortly. The crucial point to recognize is that the HO_2 radicals have their origin in (R9), while the H radicals are built up from (R18), which in turn is activated by the abundance of H_2 due to its preferential diffusion.

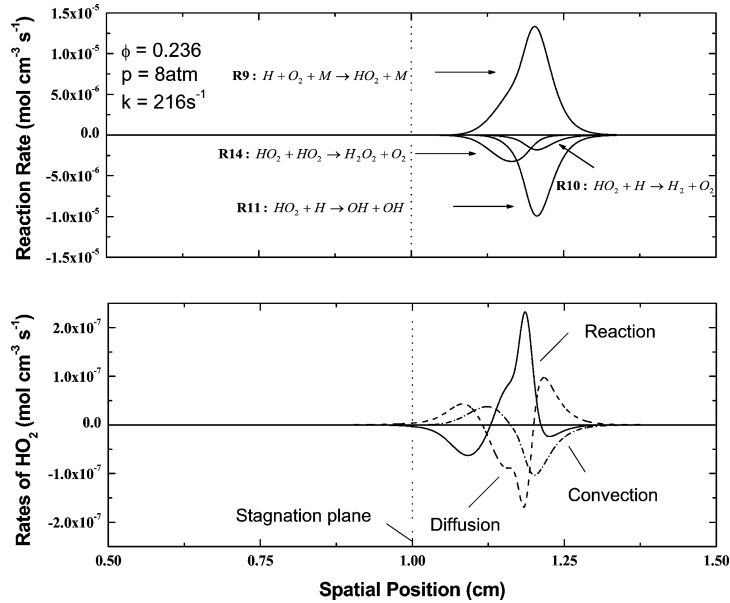


Fig. 8. Spatially resolved rates for HO₂ radical production, destruction, and mass transport (mol cm⁻³ s⁻¹) at 8 atm. Top: Rates of individual elementary reactions. Bottom: Rates of diffusive and convective transport compared with the overall chemical production rate.

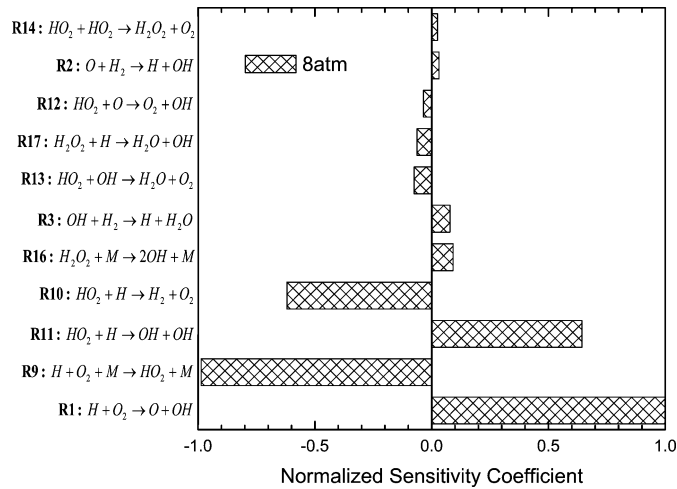


Fig. 9. Sensitivity of the S curve to individual reaction rates normalized by the largest value at 8 atm. Conditions: heated N₂ flowing against a cold mixture of 9% H₂ in air (φ = 0.236) and k = 216 s⁻¹.

Compared to the above two reactions for HO₂ consumption, (R10) and (R11), the third pathway of (R14) (HO₂ + HO₂ → H₂O₂ + O₂) and (R16) is less crucial to ignition. This is due to the fact that, since the rate of (R14) peaks closer to the stagnation plane, compared with (R11) (Fig. 8), H₂O₂, together with OH, is generated in a lower temperature region. Furthermore, some H₂O₂ generated by (R14) will be lost by mass transport. As a consequence, the above pathway has a very low efficiency at the fourth ignition

limit. The sensitivity result of Fig. 9 confirms this observation, showing (R10) and (R11) respectively having significant negative and positive effects on ignition at 8 atm, while (R16) is relatively less important.

Given the above flux and sensitivity analyses, the ignition temperature at the fourth ignition limit can be estimated by using a six-step skeletal mechanism, involving (R1), (R2), (R3), (R9), (R10), and (R11). For this mechanism the reaction rates for H, O, OH

and HO₂ are given by

$$\frac{d[\text{OH}]}{dt} = k_1[\text{H}][\text{O}_2] + k_2[\text{O}][\text{H}_2] - k_3[\text{OH}][\text{H}_2] + 2k_{11}[\text{HO}_2][\text{H}], \quad (1)$$

$$\frac{d[\text{O}]}{dt} = k_1[\text{H}][\text{O}_2] - k_2[\text{O}][\text{H}_2], \quad (2)$$

$$\frac{d[\text{HO}_2]}{dt} = k_9[\text{H}][\text{O}_2][\text{M}] - (k_{10} + k_{11})[\text{HO}_2][\text{H}], \quad (3)$$

$$\frac{d[\text{H}]}{dt} = -k_1[\text{H}][\text{O}_2] + k_2[\text{O}][\text{H}_2] + k_3[\text{OH}][\text{H}_2] - k_9[\text{H}][\text{O}_2][\text{M}] - (k_{10} + k_{11})[\text{HO}_2][\text{H}]. \quad (4)$$

The flux analysis shows that H, O, OH, and HO₂ can be considered to be in “steady state” in that their chemical creation and destruction rates are significantly higher than their characteristic rates of mass transport in the ignition kernel. This is also reflected by their concentration profiles, which lie within the ignition kernel, away from the stagnation surface as shown in Fig. 10. Furthermore, although the H profile still has a long tail extending to the hot side, the diffusion rate of H is almost 2 orders of magnitude smaller than the peak reaction rates. Since the diffusive loss of H is less significant, it is reasonable to assume that H is in steady state.

Setting Eqs. (1)–(4) to zero based on the above assumption, the following relation is obtained:

$$2k_1 = \frac{2k_{10}}{k_{10} + k_{11}} k_9[\text{M}]. \quad (5)$$

Similar to the crossover temperature, this approximate expression for the fourth limit temperature depends only on chemistry and hence can be readily evaluated. Figure 11 shows that the approximation

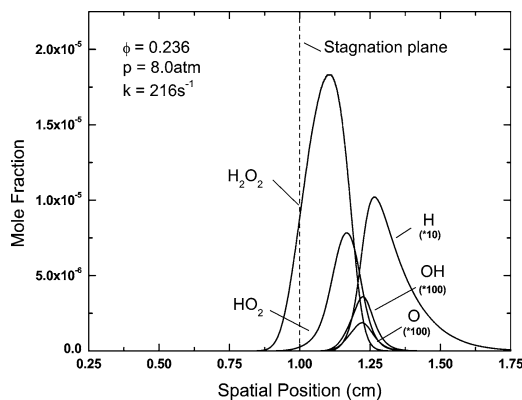


Fig. 10. Minor (H, O, OH, HO₂, and H₂O₂) species concentrations profiles at 8 atm.

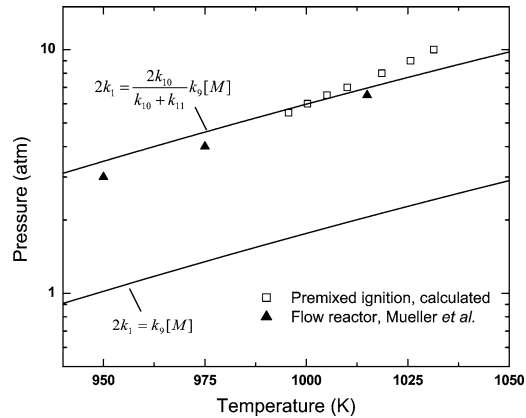


Fig. 11. Pressure-vs-temperature limits for the crossover temperature and the extended second limit. Symbols: squares are the calculated ignition temperatures for premixed counterflow (fuel side, 9% H₂ in air; hot side, N₂); triangles are the experimental data from Mueller et al. [5] for 1.0% H₂/0.5% O₂/N₂ mixture explosion limit in flow reactor experiments.

tracks the detailed calculation quite well, with the deviation increasing at higher pressures because the pathways of (R14) and (R16) can no longer be neglected.

Compared to the expression for the classical crossover temperature, $2k_1 = k_9[\text{M}]$, which describes the second explosion limit, the factor $2k_{10}/(k_{10} + k_{11})$ in Eq. (5) can be considered to play the role of modifying the chain termination rate k_9 . It accounts for the extent to which HO₂ is fully terminated through (R10), compared to the remaining fraction that becomes part of the branching pathway through (R11). Since both calculation and flux analysis showed that k_{10} is always less than k_{11} , this factor is less than unity and therefore effectively reduces the influence of k_9 . Consequently, at a given pressure the present, fourth ignition limit is shifted to lower temperatures compared to the crossover temperature.

It is also of particular interest to note that the expression just derived for this limit, Eq. (5), follows closely the extended second limit in the flow reactor studies of Ref. [5], as shown in Fig. 11. To explore the correspondence in ignition between the present premixed counterflow and the flow reactor, an ignition calculation using SENKIN [16] was performed for a 1.0% H₂/0.5% O₂/N₂ mixture with the initial condition of 8 atm and 1050 K, which correspond to a case for the extended second limit predicted by Ref. [5]. The generation and destruction rates of HO₂ radicals as a function of time are plotted in Fig. 12, which shows that, similar to the counterflow ignition, once HO₂ is generated by (R9), it will further react with H through the pathways (R10) and (R11) to influence ignition. In other words, the same group of reactions

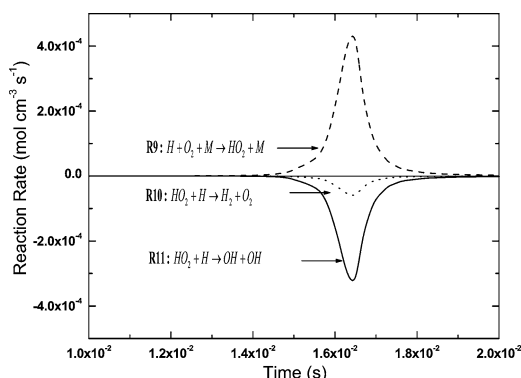


Fig. 12. The generation and destruction rates of HO_2 radicals as a function of time for a 1.0% $\text{H}_2/0.5\% \text{O}_2/\text{N}_2$ mixture with the initial condition of 8 atm and 1050 K.

controls ignition in the counterflow and explosion in the flow reactor.

Mechanistically, the classical third explosion limit observed in static reactor experiments is a consequence of the combined chemical and thermal activation in that the heat release from some slow reactions can bring the mixture to an explosion condition [5]. However, for both flow reactor and counterflow experiments, the limited residence time does not allow observation of reactions with longer characteristic times. Furthermore, extensive dilution of the mixture by nitrogen also greatly limits self-heating from these slow reactions. Consequently, the extended second limit of the flow reactor and the fourth ignition limit of the counterflow can exist at a high-temperature regime compared to the third explosion limit.

In view of the above discussion, it is reasonable to identify Eq. (5) as an explicit expression for the extended second limit of Ref. [5], with the simultaneous recognition of the importance of the HO_2 pathway, (R10) and (R11), at this limit. Following the designations for the crossover temperature and the extended second limit, it is therefore appropriate to call this expression the *extended crossover temperature*, with the understanding that, similar to the crossover temperature, the pressure–temperature range over which it holds is system dependent even though the expression itself is system independent.

3.1.4. The fifth ignition limit

The fifth ignition limit, shown in Fig. 1, is the highest pressure regime over which the ignition temperature decreases with increasing pressure. Kinetically, as the pressure increases, more and more HO_2 is generated through (R9), and its recombination reaction (R14), whose reaction rate increases quadratically with the HO_2 concentration,

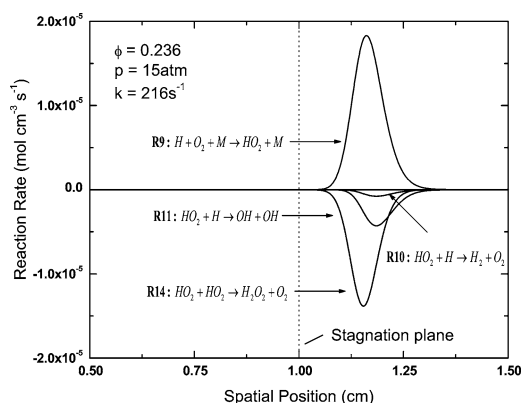
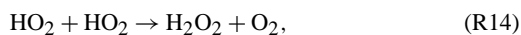
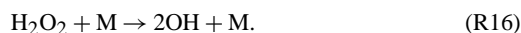


Fig. 13. Spatially resolved rates for HO_2 radical production, destruction by individual elementary reactions ($\text{mol cm}^{-3} \text{s}^{-1}$) at 15 atm.

can no longer be neglected. Due to the fact that less HO_2 is generated within the ignition kernel in the premixed case because of O_2 starvation, higher pressures are needed for (R14) to become important. As shown in Fig. 13, most of the HO_2 radicals are consumed by (R14). To a lesser extent, HO_2 will react with H through (R10) and (R11) as shown in Fig. 13. Note that some H_2O_2 radicals generated by (R14) will further decompose to two OH within the ignition kernel through (R16):



Although (R10) still functions as a chain termination step, other reactions with much higher reaction rates, i.e., (R14) (through (R16)) and (R11), are chain branching. Consequently, the ignition curve turns again and ignition becomes easier at very high pressures due to the overall chain branching characteristic. As a whole, the premixed ignition response in the fifth ignition limit is qualitatively similar to the third explosion limit for the homogeneous mixture in the sense that HO_2 becomes part of the chain propagation route, except it occurs at higher pressures with different reactions.

3.2. Effects of aerodynamic straining

Since the premixed ignition system intrinsically suffers the diffusive loss of H to the inert side, aerodynamic straining is expected to exert a significant influence on the system ignitability. To quantify this influence, the response of the ignition temperature was experimentally and computationally determined for varying flow rates and pressures. The results are plotted in Fig. 14 and discussed in the following.

First, increasing the strain rate uniformly increases the ignition temperature at all pressures because of the

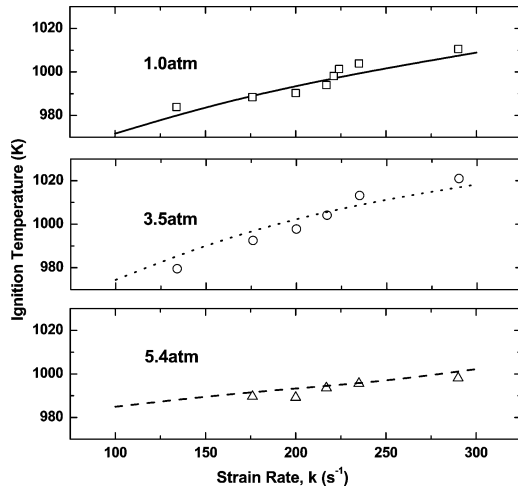


Fig. 14. Ignition temperatures vs strain rate at three different pressures. Experiments shown as symbols, and calculations shown as lines.

reduction in the residence time, which is the reciprocal of the flow strain rate [17]. Second, the ignition temperature at the fourth ignition limit, as at 5.4 atm, is less sensitive to the strain rate than that at the other two pressures shown in Fig. 14. To understand this behavior, we note that in the study of Ref. [14] at 1 atm, the rates of H production and consumption in premixed ignition were found to be of the same order as that for diffusive loss. Since a minimum radical

pool is needed for kinetic runaway to occur, higher ignition temperatures are needed such that chemical production can overcome the transport loss. If we apply this argument to the case of 3.5 atm, and since the generation and consumption rates of H atoms are now an order higher than the mass transport rates (Fig. 5), the ignition temperature should be less sensitive to the strain rate than the response at 1 atm. This, however, is not the case, as shown in Fig. 14. The reason is that not only the H radicals but also the HO₂ radicals are critical to ignition because (R18) involving HO₂ is one of the main sources in the production of the H radicals. It can be seen from the flux analysis in Fig. 15 that the rates of individual HO₂ production and consumption reactions are of the same order as that for mass transport. Furthermore, the bottom of Fig. 15 shows that convection is more important than diffusion in transporting HO₂ out of the ignition kernel. It is in this manner that convective transport plays a critical role in the third ignition limit. As a result, the ignition temperature strongly depends on the convective residence time and thereby the strain rate.

For the fourth ignition limit, as discussed earlier, H, O, OH, and HO₂ are in steady state in that their chemical creation and destruction rates are significantly larger than the characteristic rates of mass transport in the ignition kernel at higher pressures. Furthermore, although the concentration of H₂O₂ is substantially affected by mass transport, the pathway involving H₂O₂ plays a minor role on ignition. Con-

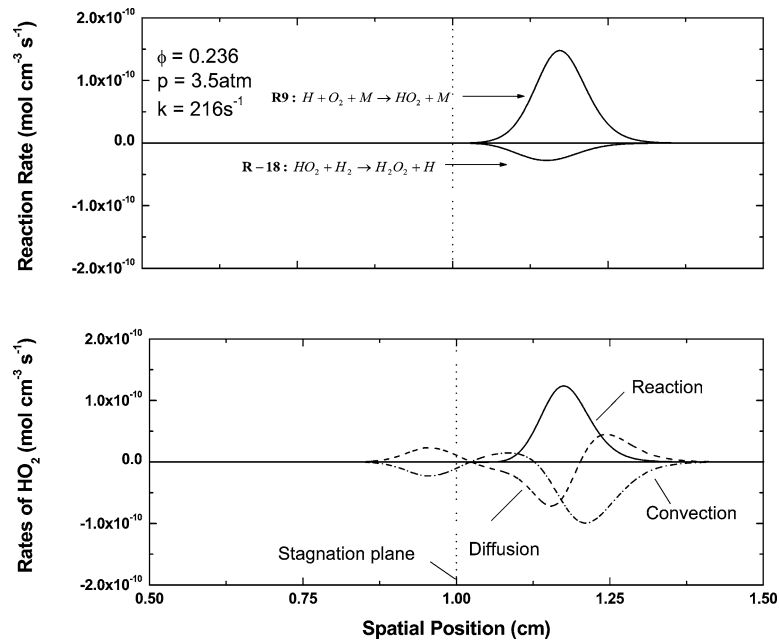


Fig. 15. Spatially resolved rates for HO₂ radical production, destruction, and mass transport (mol cm⁻³ s⁻¹) at 3.5 atm. Top: Rates of individual elementary reactions. Bottom: Rates of diffusive and convective transport compared with the overall chemical production rate.

sequently ignition at the fourth limit is strongly chemistry controlled and therefore is less sensitive to the strain rate.

3.3. Effects of O_2 doping in the hot stream

Results from the present study as well as those of Ref. [14] show that, because of the concentration stratification of the reactants in the premixed system and the subsequent loss of hydrogen to the hot stream, premixed ignition temperatures are substantially higher than those of the nonpremixed system. Ref. [14] subsequently found that the ignition temperatures can be significantly lowered by adding a small amount of oxygen to the hot stream. The viability of this possibility is further explored for its dependence on the system pressure. Figure 16 shows the experimental and calculated ignition temperatures as a function of pressure, with the O_2 mole fraction at the hot boundary being 0, 1, and 3%, respectively. A particularly interesting result is that the ignition response curve changes from five limits at 0% doping to three limits at 3% doping. This behavior is explained in the following.

For the first and second ignition limits, which occur when the pressure is below 3 atm, ignition is facilitated by replacing the inert N_2 in the hot boundary by O_2 . The effect is significant even with a small amount of O_2 addition, for two reasons. First, without O_2 in the hot free stream, the amount of oxygen within the ignition kernel is very small because it can be brought there only through diffusion across the stagnation plane against convection from the inert side. On the other hand, when O_2 is present in the hot stream, it can be brought to the ignition kernel through both convection and diffusion. The effect is therefore much larger. Second, the potential diffusive loss of H from the center of the ignition kernel is now

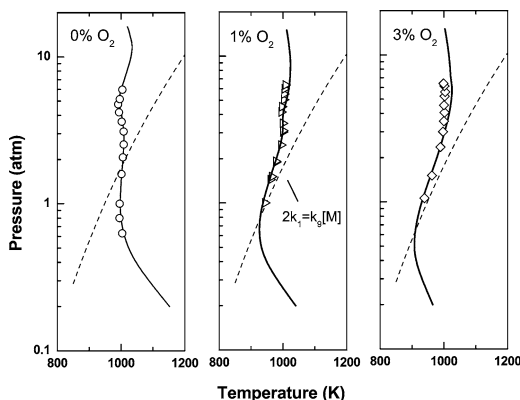


Fig. 16. Constant pressure-weighted strain rate curve of ignition temperature vs pressure for different amount of O_2 addition to the hot inert side of the flow.

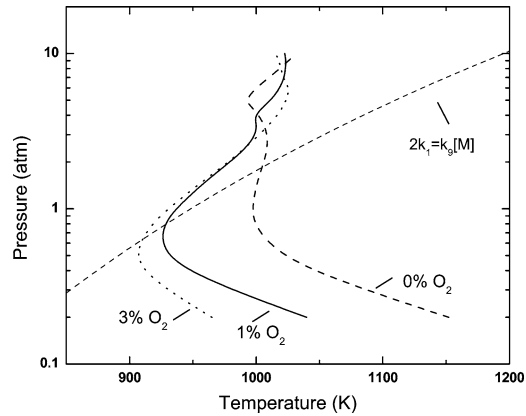


Fig. 17. Consolidated plot for the calculated results of Fig. 16 for comparison of their response to the extent of oxygen doping and pressure variation.

either significantly reduced or even practically eliminated because it is recaptured by reacting with the O_2 from the hot stream. The combination of these two factors therefore enables the critical radical concentration for ignition to build up at a lower temperature for the O_2 -doped hot stream.

The above effect, however, is weakened with increasing pressure. As shown in Fig. 17, which compares the calculated results shown in Fig. 16, the difference between the ignition temperatures becomes smaller as pressure increases. This is reasonable because the diffusive loss of H is reduced at higher pressures such that the effect of recapturing H discussed above is less significant.

When the pressure is higher than 3 atm, the second ignition limit of the O_2 -doped system terminates at a higher pressure, and the extended second limit behavior gradually vanishes. As discussed earlier, it is reaction (R18) that assists ignition by converting the relatively inert HO_2 to H at the third ignition limit. However, as more O_2 becomes available in the ignition kernel, most of the H_2 will react with O_2 instead of HO_2 . As a result, the HO_2 concentration is built up at a lower pressure and its recombination contributes to ignition at an early stage. Consequently, instead of evolving into the third, fourth, and fifth ignition limits, the O_2 -doped system will march along the third limit in the same manner as that for the homogeneous ignition.

4. Conclusions

Ignition of lean premixed hydrogen/air by heated nitrogen or a mixture of nitrogen and oxygen was studied in a laminar counterflow over a range of pressures and strain rates. Compared to the homo-

geneous explosion limits, two important distinctions were identified for the premixed ignition system. First of all, the counterflow ignition response curve is shifted to higher temperatures compared to that of the homogeneous explosion limits due to the reduced residence time as well as the additional transport loss of the H radicals. Furthermore, the omnidominance of the crossover temperature chemistry constrains the shifting to be along its p - T response path. Second, the ignition temperature was found to exhibit five limits over the pressure range investigated. The first three limits mimic the homogeneous case, except that the pronounced H radical loss to the hot inert side pushes the first limit to end at a higher pressure. The steepening of the second limit, which turns and forms the third limit, is due to the increasing importance of (R18). This reaction converts the relatively inert HO₂ to the more reactive H radical and is greatly facilitated by the abundant H₂ within the ignition kernel owing to its preferential diffusion over O₂. As the concentration of the H radical is built up through (R18) with increasing pressure, reactions between HO₂ and H ((R10) and (R11)) start to be important and exert a retarding influence on ignition. The resulting fourth ignition limit resembles the previously observed extended second explosion limit from flow reactor studies and can be described by the classical crossover temperature expression with k_9 modified and thereby weakened by the factor $2k_{10}/(k_{10} + k_{11})$. The final, fifth limit is characterized by the self-recombination of HO₂ through (R14) and as such describes the high-pressure regime of the third explosion limit. As a whole, the third, fourth, and fifth ignition limits can be interpreted as a punctuated manifestation of the third explosion limit in that the third and fifth ignition limits would correspond to the third explosion limit at lower and higher pressures, respectively, with their transition interrupted by the fourth limit, which is a reemergence of the second limit moderated by the partial reactivation of the HO₂ through its reactions with H.

We have also shown that aerodynamic straining increases the ignition temperature, which is reasonable because of the reduced residence time, although the response is less sensitive at the extended second limit, which is mostly chemistry controlled. Furthermore, oxidizer doping in the inert flow moderates the extent of H leakage and the various consequences of the preferential diffusion of H₂ such that the ignition

response is again characterized by three limits similar to those of homogeneous explosion and nonpremixed ignition.

Acknowledgments

This research was supported by the Army Research Office, under the technical monitoring of Dr. David Mann, and a center grant on carbon mitigation sponsored by the British Petroleum Corp.

References

- [1] G. Von Elbe, B. Lewis, *Combustion, Flames, and Explosions of Gases*, 3rd edition, Academic Press, Orlando, FL, 1987.
- [2] J. Warnatz, in: W.C. Gardiner Jr. (Ed.), *Combustion Chemistry*, Springer-Verlag, New York, 1984, pp. 197–360.
- [3] R.A. Yetter, F.L. Dryer, H. Rabitz, *Combust. Sci. Technol.* 79 (1991) 97–128.
- [4] T.J. Kim, R.A. Yetter, F.L. Dryer, *Proc. Combust. Inst.* 25 (1994) 759–766.
- [5] M.A. Mueller, T.J. Kim, R.A. Yetter, F.L. Dryer, *Int. J. Chem. Kinet.* 31 (1998) 113–125.
- [6] N. Darabiha, S. Candel, *Combust. Sci. Technol.* 86 (1992) 67–85.
- [7] T.G. Kreutz, M. Nishioka, C.K. Law, *Combust. Flame* 99 (1994) 758–766.
- [8] G. Balakrishnan, M.D. Smooke, F.A. Williams, *Combust. Flame* 102 (1995) 329–340.
- [9] C.G. Fotache, T.G. Kreutz, D.L. Zhu, C.K. Law, *Combust. Sci. Technol.* 109 (1995) 373–394.
- [10] T.G. Kreutz, C.K. Law, *Combust. Flame* 104 (1996) 157–175.
- [11] T.G. Kreutz, C.K. Law, *Combust. Flame* 114 (1998) 436–456.
- [12] C.G. Fotache, C.J. Sung, C.J. Sun, C.K. Law, *Combust. Flame* 112 (1998) 457–471.
- [13] J.D. Blouch, C.J. Sung, C.G. Fotache, C.K. Law, *Proc. Combust. Inst.* 27 (1998) 1221–1228.
- [14] X.L. Zheng, J.D. Blouch, D.L. Zhu, T.G. Kreutz, C.K. Law, *Proc. Combust. Inst.* 29 (2002) 1637–1644.
- [15] I. Glassman, *Combustion*, 3rd edition, Academic Press, San Diego, CA, 1996.
- [16] M.J. Day, K. Thompson, G. Dixon-Lewis, *Proc. Combust. Inst.* 14 (1972) 47–59.
- [17] H. Schlichting, *Boundary Layer Theory*, McGraw-Hill, New York, 1979, p. 95.